2019

Experimental characterization of wildfire sprinkler sprays using high-speed videography

Alan Green
University of Wollongong, alang@uow.edu.au

Paul Cooper
University of Wollongong, pcooper@uow.edu.au

Experimental characterization of wildfire sprinkler sprays using high-speed videography

Abstract

External sprinkler systems are one of a relatively small number of measures that are frequently recommended for the protection of houses from wildfires. However, very little scientific work appears to have been undertaken to evaluate their effectiveness. Numerical simulation techniques such as computational fluid dynamics (CFD) could be used to investigate spray performance in the conditions of a wildfire; however, detailed characteristics of the sprays typically implemented in wildfire sprinkler systems must first be known so that they can be accurately represented in such simulations. This paper presents the results of an in-depth experimental investigation into the spatiotemporal distributions of droplet mass flux, diameter, and velocity in six water sprays used in wildfire sprinkler systems. The sprays were produced using (1) a flat-fan misting nozzle, (2) a hollow-cone nozzle, (3) a deflector-plate sprinkler, (4) a butterfly sprinkler, (5) an impact sprinkler main nozzle, and (6) the auxiliary nozzle of the same impact sprinkler. The experimental and video-analysis methodologies developed have also been described in detail, to serve as a guide for future investigations. A single-camera, back-illuminated, high-speed videography technique was adopted, and droplets within a specific measurement volume were identified in the video footage using a focal criterion based on the point-spread function half-width of droplet images. A new technique was developed to separate overlapping droplet images, which was found to perform better than existing methods when applied to noncircular droplet images. Procedures for the tracking of droplets between video frames and statistical correction of sampling biases are also described in detail.

Disciplines

Engineering | Science and Technology Studies

Publication Details

Green, A. & Cooper, P. (2019). Experimental characterization of wildfire sprinkler sprays using high-speed videography. Atomization and Sprays, 29 (5), 381-402.

Experimental Characterisation of Wildfire Sprinkler Sprays using High-Speed Videography

Alan Green*[1] and Paul Cooper[1]

[1] *Sustainable Buildings Research Centre, University of Wollongong, Australia*

**Corresponding author: alang@uow.edu.au; Sustainable Buildings Research Centre, bld. 237, University of Wollongong, Wollongong, NSW, Australia, 2522.*

Abstract

External sprinkler systems are one of a relatively small number of measures that are frequently recommended for the protection of houses from wildfires. However, very little scientific work appears to have been undertaken to evaluate their effectiveness. Numerical simulation techniques such as computational fluid dynamics (CFD) could be used to investigate spray performance in the conditions of a wildfire; however, detailed characteristics of the sprays typically implemented in wildfire sprinkler systems must first be known, so that they can be accurately represented in such simulations.

This paper presents the results of an in-depth experimental investigation into the spatiotemporal distributions of droplet mass flux, diameter and velocity, in six water sprays used in wildfire sprinkler systems. The sprays were produced using: a flat-fan misting nozzle, a hollow-cone nozzle, a deflector-plate sprinkler, a butterfly sprinkler, an impact sprinkler main nozzle, and the auxiliary nozzle of the same impact sprinkler.

The experimental and video-analysis methodologies developed have also been described in detail, to serve as a guide for future investigations. A single-camera, back-illuminated, high-speed videography technique was adopted, and droplets within a specific measurement volume were identified in the video footage using a focal criterion based on the point-spread function half-width of droplet images. A new technique was developed to separate overlapping droplet images, which was found to perform better than existing methods when applied to noncircular

droplet images. Procedures for the tracking of droplets between video frames and statistical correction of sampling biases are also described in detail.

Keywords: bushfire, fire safety, wildland-urban interface, image analysis, particle tracking velocimetry, point-spread function, irrigation.

1 Introduction

The hazard posed by wildfires to human lives and property is significant and increasing, as urban expansion increases the number of exposed buildings, and the severity and frequency of wildfires are increased by global warming (Lucas *et al.*, 2007; Krawchuk *et al.*, 2009; Syphard *et al.*, 2013; Moritz *et al.*, 2014; Bowman *et al.*, 2017). External water spray systems have been promoted by several fire protection agencies in Australia and the USA as an effective means to protect buildings from wildfire when implemented alongside other protective measures (FPAA, 2000; Mitchell, 2006; FEMA, 2008; Potter and Leonard, 2010; CFS, 2011; Standards Australia, 2012). However, very little scientific evidence that quantifies wildfire sprinkler effectiveness appears to have been published.

Scientifically rigorous investigation of wildfire sprinkler performance is not straight-forward, due to the complex interactions that occur between the sprays, wind, fire and buildings; which cannot easily be reproduced in experiments. Numerical methods, such as computational fluid dynamics (CFD), could be suitable for such investigations, but require validation against experimental data for them to be deemed accurate or reliable. Detailed and accurate near-nozzle spray data is needed for such CFD simulations, to form the basis of spray boundary conditions if the sprays are to be modelled as sets of pre-formed droplets, or be used to form or validate atomisation models if they are to be used to set droplet initial conditions (Yoon *et al.*, 2007; Myers and Marshall, 2016).

Various and conflicting recommendations have been previously given as to the types of sprinklers that should be utilised in wildfire sprinkler systems. 'Butterfly' and 'impact' sprinklers, such as those typically used for garden irrigation, have been recommended by several fire agencies (FPAA, 2000; GTVFD, 2007; CFS, 2011). However, such sprinklers do not comply with the Australian Standard on wildfire sprinkler system design, which stipulates that sprinklers must not contain any moving parts (Standards Australia, 2012). 'Pendant' and 'upright' sprinklers, similar to those designed for indoor fire sprinkler systems, have also been recommended (FPAA, 2000), as have fine hollow-cone sprays (Mitchell, 2006). A detailed survey of 13 existing wildfire sprinkler systems was reported by the Fire Protection Association Australia (FPAA, 2000), in which misting nozzles, butterfly sprinklers, impact sprinklers and pendant/upright sprinklers were all documented. Johnson *et al.* (2008) also reported on 56 existing systems, which appear to have all used impact sprinklers, on the advice of the local wildfire brigade.

Several previous studies have characterised sprays that may be relevant to wildfire sprinkler systems. Detailed measurements of droplet sizes and velocities produced by an impact sprinkler have been published by Bautista-Capetillo *et al.* (Bautista-Capetillo *et al.,* 2009, 2014; Salvador *et al.*, 2009). However, these measurements were taken at ground level, to evaluate the properties of droplets impacting on crops during spray irrigation, so they do not provide the droplet 'initial' conditions required for CFD simulations. Other previous studies have experimentally characterised sprays that have not been specifically documented in wildfire sprinkler literature but could be appropriate for use in such systems, such as flat-fan, hollow-cone and solid-cone sprinklers intended for pesticide application (Sidahmed *et al.*, 2005; Guler *et al.*, 2007, 2012; Nuyttens *et al.*, 2007; Dorr *et al.*, 2013; Vulgarakis Minov *et al.*, 2016), and misting, upright and pendant indoor fire sprinklers (You, 1986; Widmann *et al.*, 2001; Everest and Atreya, 2003; Sheppard and Lueptow, 2005; Santangelo, 2010; Ren *et al.*, 2011; Yoon *et*

al., 2011; Zhou *et al.*, 2012, 2014). While these existing datasets could assist CFD practitioners in accurately simulating such sprinklers, detailed near-nozzle characteristics of the sprays produced by some of the most commonly documented wildfire sprinklers (e.g. butterfly and impact sprinklers) do not appear to have been published previously.

This paper reports on the detailed experimental characterisation of six sprays typical of those documented in wildfire sprinkler literature. Detailed descriptions of the sprinklers are provided in Section 2, the experimental and data analysis methodologies, including several novel techniques, are described in Section 3, and results from the measurements are presented and discussed in Section 4.

2 Sprinklers investigated

The brass sprinklers used to produce the six sprays characterised in the present study are described in Table 1 and depicted in Figure 1. Each sprinkler was operated at one supply pressure within the range recommended by the device manufacturers (see Table 1), and was new at the time of measurement (i.e. not previously used in service).

The butterfly sprinkler used to produce Spray B ejected water through a 6.5 mm circular orifice onto an asymmetric scooped deflector, which was free to rotate about the y-axis. The flat-fan and deflector plate sprinklers emitted continuous liquid sheets, formed as cylindrical water jets (of 1.8 and 8mm-diameter, respectively) impinged on deflector surfaces on the sprinklers, which were atomised a short distance from each sprinkler. A conical liquid sheet was formed by the hollow-cone sprinkler, as water was emitted through an annular orifice with outer and inner diameters of 8 mm and 4.5 mm, respectively. Spray IM was produced from a 4.4 mm-diameter cylindrical liquid jet that was intermittently interrupted by a swinging deflector paddle, and spray IA was formed by a 2.4 mm cylindrical jet that impinged on the inside of a short, 5 mm-diameter chamber, with a 1.5 mm slot machined along one side. Both spray IM

and spray IA had a relatively slow, incremental, rotation about the y-axis, driven by the deflector paddle, which imparted an impulse on the impact sprinkler head with every oscillation.

3 Method

The characterisation procedure involved: the verification and calibration of the video analysis procedure using droplets and discs of known diameter, videography of the six sprays, and analysis of the video footage. A custom image analysis and droplet tracking program was developed using Matlab (version R2016a), to automate the video analysis procedure.

3.1 Videography

Each spray was operated individually within a 3.0 m × 1.8 m × 2.4 m (high) enclosure, as shown in Figure 2. The enclosure was used to confine water from the sprays, recirculate it to the supply pump and exclude light other than that which was introduced deliberately as back-lighting. Water was supplied to the sprinklers by a centrifugal pump, via a Trimec TF015 positive-displacement flow meter, pressure regulator and Wika analogue pressure gauge. The regulator was adjusted manually, to maintain water supply pressures within ±5% of the values reported in Table 1.

Back-illumination was provided to the sprays by four 185 W LED lights, which projected light into the test enclosure through an optical diffuser. A constant d.c. voltage was supplied to the lights, to avoid flicker in the high-speed footage. Video footage was generated using a single Vision Research Phantom v611 high-speed camera, fitted with a Tamron 90 mm f/2.8 macro lens set to its maximum aperture. The sprays were videoed through a window opposite the light source, producing silhouette images of droplets within the sprays.

Videos of many partially overlapping regions were recorded within each spray, at a specific distance from the sprinkler, beyond the primary breakup region. Thus, a series of videos

provided a record of droplets formed within a thin, pseudo-planar 'slice' of the spray. The camera settings and position of the sprinkler relative to the camera were optimised to suit the different spray patterns, breakup lengths, and droplet sizes and velocities of each spray (see Table 2). Sprays HC, DP and B were assumed to be approximately axisymmetric about the y-axis when time-averaged, and spray FF was assumed to be symmetric about the xy-plane.

The liquid jet that formed spray IM when undisrupted by the deflector paddle was observed to break up over a relatively long distance; many water sheets and ligaments remained intact at a distance of 4 m from the sprinkler. Such structures were not well-suited for image analysis, and did not represent the fully atomised spray that was of interest, so the undisrupted spray IM was measured at the relatively large distance of 6 m from the sprinkler. The sprinkler was tilted forwards by 15° during these measurements, in order to place the spray within the camera field of view.

3.2 Model Calibration and Verification

Videos were recorded of opaque discs and individual droplets of known diameter in the test enclosure to verify the dimensional accuracy of the image analysis and develop the correlations used as focal criteria for the spray footage. The droplets and discs were positioned at a range of known distances in front of and behind the focal plane of the camera, and this process was repeated at each of the two chosen experimental 'working distances'.

The opaque discs came etched on a glass Pyser PS20 universal calibration slide, and ranged in diameter from 0.15 mm to 3.5 mm. Droplets were generated using a piezoelectric-actuated drop-on-demand generator and three 'dropper' nozzles of different sizes, which were supplied with a constant flow of water using a syringe pump. When supplied with water, the drop on demand generator and nozzles reliably produced droplets with diameters of 0.047, 1.58, 3.17 and 4.57 mm. The smallest dropper nozzle was also fed with a mixture of methanol and water,

in a volume ratio of 80% methanol to 20% water, which produced 1.28 mm droplets. These droplets had a similar refractive index to water (Herráez and Belda, 2006) but were smaller than droplets that could be formed by dropper nozzles using water, due to the significantly lower surface tension of the methanol-water mixture (Vazquez *et al.*, 1995).

3.3 Image Analysis

Individual video frames from the spray and calibration measurements were analysed, to locate and measure individual droplet images. The method adopted for this analysis was modelled closely on that of Blaisot *et al.* (Malot and Blaisot, 2000; Blaisot and Yon, 2005; Fdida and Blaisot, 2010; Blaisot, 2012), with some new techniques, developed to suit the relatively large non-spherical droplets in this study.

A 'background' image was formed by taking the average of 20 video frames obtained using the same camera and lighting settings, but with no spray in view. The frame under analysis was then normalised, by dividing the intensity of each pixel by the corresponding 'background' value, and converted to grey-scale. Droplet images were located within each frame using an intensity threshold of 0.3, and by convoluting the image with three inverted 'Mexican hat' (i.e. Laplacian of Gaussian) wavelet functions, each with a different width. The union of regions identified by these methods formed a set of 'blobs', which corresponded to regions in the frame that were dark or had a highly 'concave' intensity profile.

Blobs that touched the border of the frame or were comprised of less than 3 pixels were disregarded, and regions of the image corresponding to the remaining blobs were then analysed as individual droplets (see Figure 3). A bilinear sub-pixel interpolation was performed on a region encompassing the droplet image, and any regions within this smaller image that corresponded to other blobs were masked. The droplet image local contrast was defined as the difference between the mean local background intensity and the image minimum intensity, and

the droplet boundary was defined as the contour of intensity halfway between those extremes. For more details on this process, the interested reader is directed to Fdida and Blaisot (2010).

Some droplet images overlapped, such that their boundaries were erroneously combined. Methods that had previously been used to automatically detect and separate overlapping droplet images utilising the boundary shape, including watershed algorithms (Castanet *et al.*, 2013), the Hough transform (Lee and Kim, 2004) and the division of droplet images between points of high boundary curvature (Fdida and Blaisot, 2010; Blaisot, 2012; Castanet *et al.*, 2013), were trialled but performed poorly when applied to the non-circular droplet images that were common in this study. In response to these issues, a new image separation method was developed, based on the spatial rate of change in intensity gradient along the image boundary. It involved the five steps outlined below and is depicted in Figure 4.

1. Identification of potential 'break points', by calculating the intensity gradient at each pixel on the image boundary, smoothing and fitting a spline to the profile formed by these values, and identifying peaks in the absolute value of the derivative of the spline. Peaks that exceeded a threshold, τ_s, were considered as potential break points, and images with more than two potential break points were treated as the overlapping images of multiple droplets. The threshold τ_s was tuned to suit each spray.
2. Calculation of the mean point-spread function (PSF) half-width of each boundary segment. The PSF half-width is a measure of image defocus, which was calculated using methods described by Blaisot (2012).
3. Definition of secondary break points, translated along the combined image boundary from each of the original break points, towards the boundary segment in poorer focus, by a distance ⅔ times the PSF half-width of the boundary segment in poorer focus.
4. Completion of each droplet image boundary by joining each pair of break points with an arc (Figure 4). The arc radii were calculated from the chord length between break points

and perimeter of the boundary segment being closed, such that a circular boundary would be completed correctly.

5. Subsequent treatment of regions within each boundary as separate droplet images. Regions of overlap were included in calculations of droplet size, but were ignored in calculations of the local contrast of each image and mean intensity gradient at the image boundary.

By separating overlapping droplet images, many inaccurate measurements of droplet size and local contrast were avoided. Furthermore, overlapping image separation allowed the droplets that were involved to be tracked through frames in which overlap occurred, thereby reducing the number of droplets that were measured twice or tracked incorrectly.

Droplet volumes were estimated from the two-dimensional droplet images by: i) dividing the primary (i.e. longest) axis of the droplet image into 100 intervals, ii) measuring the image width, normal to the primary axis, at the centre of each interval, iii) taking each width measurement to represent the diameter of a cylinder, and iv) summing the cylinder volumes. The equivalent spherical diameter of each droplet was calculated from the estimated volume, and the diameter was corrected for the effects of image defocus using an empirical model, similar to that developed by Fdida and Blaisot (2010) but calibrated for the optical setups used in the present study.

In order to estimate droplet locations in the dimension normal to the imaging plane, the PSF half-width of each droplet image was calculated from the mean intensity gradient at the image boundary, using the method proposed by Blaisot (2012). Previous investigations have demonstrated an approximately linear relationship between the PSF half-width of an image and the distance of the imaged object from the focal plane. In the present work, such relationships were established for each working distance using the calibration images of discs and droplets of known location. These empirical linear equations were then used to estimate the distance of droplets within the spray footage from the focal plane. Thus, the set of measurements recorded

for each droplet image was comprised of: i) the corrected equivalent spherical diameter, ii) the horizontal and vertical coordinates of the droplet image centroid within the video frame, and iii) the estimated distance of the droplet from the focal plane.

3.4 Droplet Tracking

Droplets were tracked through sequences of video frames using a cost function-based method, modelled closely on that outlined by Dalziel (1992) and implemented for particle-tracking velocimetry in the software DigiFlow (Dalziel, 2006). Cost values were calculated for the pairing of each droplet image in one video frame to each of those in the subsequent frame, such that low cost values indicated a high likelihood that the images were of the same droplet. The cost of pairing droplet i from one frame to droplet j in the subsequent frame was given by:

$$C_{ij} = C_{loc} + C_{dia} + C_{foc} + C_{fee} \tag{1}$$

where C_{loc}, C_{dia} and C_{foc} are sub-costs related to the droplet location, diameter and focus, respectively, and C_{fee} is a 'joining fee'. The location sub-cost was defined as:

$$C_{loc} = \max\left\{ 0 , W_{loc}\left(\sqrt{\left(x_i + u_i\delta_t - x_j\right)^2 + \left(y_i + v_i\delta t - y_j\right)^2} - T_{loc}\right)\right\} \tag{2}$$

Here, W_{loc} and T_{loc} are user-defined weighting and threshold parameters, x and y are the droplet image horizontal and vertical coordinates, u and v are horizontal and vertical velocity components, subscripts i and j refer to the respective droplet images, and δ_t is the time period separating the two video frames. Velocity components u_i and v_i were the average of those established for droplet i in previous tracking steps; droplets with no velocity history (i.e. those that had not been paired with droplet images in previous frames) were assigned user-defined constant values, u_e and v_e. Two different values were set for T_{loc}, such that:

$$T_{loc} = \begin{cases} T_{loc,1} & n_i = 1 \\ T_{loc,2} & n_i > 1 \end{cases} \tag{3}$$

where n_i is the number of video frames through which droplet i had already been tracked. Thus, by setting $T_{loc,1} > T_{loc,2}$, previously unpaired droplets could be paired more readily with droplets in a relatively large region of the subsequent video frame, but the continuation of existing droplet trajectories was more heavily constrained to maintain the established velocity history.

The diameter cost was defined as:

$$C_{dia} = \max\left\{0\,, W_{dia}\left(\frac{2|d_i - d_j|}{d_i + d_j} - T_{dia}\right)\right\} \tag{4}$$

where W_{dia} and T_{dia} are user-defined diameter weighting and threshold parameters, respectively, and d is the droplet equivalent spherical diameter. The focal cost was defined as:

$$C_{foc} = \max\left\{0\,, W_{foc}\left(\frac{2|z_i - z_j|}{z_i + z_j} - T_{foc}\right)\right\} \tag{5}$$

where W_{foc} and T_{foc} are user-defined focus weighting and threshold parameters, respectively, and z is the estimated droplet distance from the focal plane.

The joining fee C_{fee} was set as zero for droplets that had been paired in previous tracking steps, and equal to a user-defined positive constant for those that had not:

$$C_{fee} = \begin{cases} F & n_i = 1 \\ 0 & n_i > 1 \end{cases} \tag{6}$$

A single fixed cost, C_0, was also defined, for the pairing of any droplet with a hypothetical 'out of view' droplet. Droplet images that could not be paired with a cost less than C_0 were paired with the 'out of view' droplet, and were assumed to have entered or exited the field of view.

The final pairing of droplet images from one frame with those in another was that which minimised the sum total cost. First, an initial feasible solution was established by progressively combining possible image pairs in order of increasing cost, until every image in both frames had been paired once; then incremental improvements were achieved by 'swapping' the two

image pairs that, if swapped, caused the greatest decrease in the sum total cost, until no such improvements could be made. This procedure was sped up substantially by only comparing image pairs with a cost less than C_0.

After droplets had been tracked between two sequential frames (say, frames p and $p+1$), an attempt was made to pair any unpaired droplet images in the second frame ($p+1$) to those that had not been tracked forward in the previous tracking step (from frame $p-1$). Thus, failure to detect a droplet in an isolated video frame did not necessarily disrupt its measurement.

It was found to be a relatively straight-forward process to tune W_{loc}, $T_{loc,1}$, $T_{loc,2}$, W_{dia}, T_{dia}, W_{foc}, T_{foc}, u_e, v_e, F and C_0 to suit each spray, resulting in accurate and reliable droplet tracking between video frames. The mean and standard deviation of several characteristics were recorded for each droplet tracked, including: i) equivalent spherical diameter, ii) velocity, iii) location relative to the sprinkler (η and ζ), and iv) distance from the focal plane.

3.5 Focal Criterion

Only droplets that had been located within a relatively narrow depth-of-field (in the order of 10mm) were analysed and tracked, since highly defocused droplet images were not detectable. However, this depth-of-field increased with droplet size. In order to remove bias towards larger droplets, and to define a distinct known measurement volume for flux calculations, a focal criterion was implemented based on the mean PSF half-width of measured droplets. Droplets determined to have been more than 1.5 mm and 3.0 mm from the focal plane were removed from measurements taken at working distances of 122 mm and 247 mm, respectively. The relationship between PSF half-width and distance from the focal plane was established for each optical setup during the calibration procedure (see Section 4.1).

3.6 Removal of Spurious Results

The automatic video analysis procedure was generally very accurate and reliable. However, a small number of spurious results were introduced by two mechanisms: i) pairing of images of different droplets during the tracking procedure, and ii) appearance of droplets in the field of view that had not originated directly from the sprinkler (e.g. those produced by splashing on surfaces in the test enclosure, or emitted by the sprinkler at a different angle and then forced into the field of view by air flow and/or gravity). Incorrect image pairs that arose in the tracking procedure predominantly involved droplet images that had not been paired with any previous images (i.e. those with no velocity history), and rarely persisted for more than one tracking step. Thus, the majority of such spurious results were removed by ignoring droplets that had been identified in 2 frames or less. Droplets that had not originated directly from the sprinkler were not always easy to identify, since they could become entrained into the induced air flow within the spray and reach velocities similar to the droplets of interest. Droplets with a direction of travel outside of an acceptable range were removed from the data, which reduced the number of spurious results. However, it is likely that some bias was introduced towards smaller droplets, since drag forces would have a relatively large effect on their trajectories, rendering them more prone to entrainment. Such issues could be mitigated in future studies by maximising the size of the test enclosure, and thereby reducing the number of splashed and recirculated droplets.

3.7 Correction for Sampling Bias

Data derived directly from the analysis outlined above did not accurately represent the distribution of droplets emitted from the sprinklers, since the streamwise spacing of slower-moving droplets is less than that of faster droplets with the same number flux. In the present study, discrete samples of sequential video frames were sampled and analysed from video footage of the sprays; slow droplets remained within the field of view for a greater number of

video frames, so were more likely to be included in a sample. The probability that a given droplet would appear in enough sampled frames to be included in the measurement was given by:

$$P_i = \frac{n_{di}+n_f-2n_{min}}{n_p} \tag{7}$$

where n_{di} is the number of frames in which droplet i was within the field of view, n_f is the number of frames included in each sample, n_{min} is the minimum number of frames with which droplets would be included (3 in the present case), and n_p is the number of frames separating the start of each sample (i.e. n_f plus the number of unsampled frames before the next sample). The number of frames in which a droplet appeared could be estimated from the droplet speed:

$$n_{di} \approx \frac{f_{FR}w_{FOV}}{S_i} \tag{8}$$

where f_{FR} is the frame rate, w_{FOV} is the width of the field of view on the focal plane and S_i is the speed of droplet i.

Another source of bias influenced measurements of the axisymmetric sprays, i.e. HC, B and DP. A larger fraction of droplets emitted close to the axis of symmetry in these sprays were within the finite depth-of-field than those emitted closer to $\eta = 0°$ (see Figure 5), and therefore were overrepresented in the datasets.

The two sources of bias mentioned above were addressed by weighting the contribution of each droplet measurement by a factor, defined as:

$$\phi_i = \frac{W_i}{P_i} \tag{9}$$

where W_i is a factor for the correction of bias in data from axisymmetric sprays, set equal to $\cos(\eta_i)$ for axisymmetric sprays and 1 for others. These weighting factors were applied in the calculation of all results presented in the present work.

3.8 Interpretation of Results

Information contained in the sets of individual droplet measurements and corresponding weighting factors included co-distributions of volume flux, diameter and speed, resolved in space, and in the cases of sprays B and IM, time. The spatiotemporally averaged characteristics of each spray were summarised using four representative diameters, a standard diameter distribution function, and a characteristic speed. The representative diameters included the arithmetic mean diameter (d_{10}), the volume mean diameter (d_{30}), the volume-length mean diameter (d_{31}), and the Sauter mean diameter (d_{32}). Four functional forms were fitted to the droplet diameter distributions measured in each spray, including the Rosin Rammler distribution, the log-normal distribution, the upper-limit log-normal distribution (Mugele and Evans, 1951), and a hybrid log-normal/Rosin Rammler distribution (You, 1986; Ren *et al.*, 2011), and whichever function fitted the data with the lowest RMS deviation was reported. The spray characteristic speed was defined as the volume-weighted mean droplet speed.

In order to communicate spatial and temporal variations in the distributions of droplet diameters and speeds within the sprays, as well as any covariance between diameter and speed, continuous distributions were formed from the discrete droplet measurements using a kernel density estimation method. 'Local' Sauter mean diameters and 'local' characteristic speeds were also calculated using a Gaussian kernel estimation method, in order to represent local droplet diameter and speed distributions using single values.

4 Results and Discussion

4.1 Model Calibration and Verification

The diameters of calibration droplets and discs, within the depths-of-field set at working distances of 122 mm and 247 mm, were measured with a mean absolute error of 2.9% and 1.3%, respectively (see results for a 122 mm working distance in Figure 6). Uncorrected

measurements of very small (47 µm) droplets were affected significantly by the degree of image focus, but the correction method, proposed by Fdida and Blaisot (2010) and adapted to the optical setup used in the present work, addressed such inaccuracy very effectively (see inset in Figure 6a). Measurements of larger droplets and discs were not affected by image defocus to such a degree, but were improved by the diameter correction model as it corrected for inaccuracy in the length scale that was initially set (to convert pixels to mm).

The relationship between PSF half-width and distance from the focal plane could be approximated very well by a linear function at each working distance, in between a central region near the focal plane where apparent image focus was influenced by image resolution, and regions of extreme defocus where PSF half-width could not be determined accurately (see Figure 7). The size of droplet or disc in the image did not influence this relationship significantly, which confirmed that the PSF-based focal criterion was able to accurately identify droplets within a distinct depth-of-field, without introducing bias towards larger or smaller droplets.

4.2 Bulk Spray Properties

The spatiotemporally averaged distributions of droplet diameters and speeds within the sprays have been plotted in Figures 8–9, and described using representative diameters and standard diameter distribution functions in Table 3. Sprays B, HC, FF, DP and IA predominantly contained droplets with diameters in the range 0.1–1.8 mm, and speeds between 2 and 22 m s^{-1}. Compared to other sprays used for fire suppression, spray B was the most similar to previously characterised ‘pendant’ and ‘upright’ sprinklers (Zhou *et al.*, 2012, 2014), while sprays FF, HC and DP were comprised of smaller droplets, and sprays FF, IA and DP expelled droplets at higher velocities. Sprays FF, HC and DP contained droplets small enough to be considered water mists in current fire protection standards (Standards Australia, 1999; ISO, 2005; NFPA, 2010).

Many large (~5 mm) droplets were recorded in spray IM when it was not disrupted by the deflector paddle, which influenced the volume-weighted diameter distribution of this spray significantly. It is likely that such large droplets would have undergone secondary breakup further downstream. Therefore, the characteristics presented here for spray IM in its undisrupted mode represent a compromise between the fully atomised characteristics that occur too far downstream to be useful as boundary conditions in simulations, and characteristics of the liquid jet close to the sprinkler which lack information on the droplet sizes and velocities that arise through atomisation. None of the standard diameter distribution functions fitted data from this spray accurately, so they have not been reported.

4.3 Spatiotemporal Variations

Significant spatial variations were measured in the droplet mass flux, diameter and speed distributions within the sprays (see Figures 10–15). Typically, high concentrations of relatively large, fast droplets were observed in central regions of the sprays, surrounded by smaller, slower droplets. The two notable exceptions to this distribution were: i) the relatively large, slow droplets formed at the edges of liquid sheets emitted from the flat-fan and auxiliary impact sprinkler nozzles, and ii) droplets towards the centre of the hollow-cone spray pattern, which were not significantly slower than those in more dense regions of the spray.

The oscillatory action of the butterfly and impact sprinklers also gave rise to significant temporal variations in sprays B and IM. Rotation of the impact sprinkler head about the y-axis occurred with a mean period of 27.7 s, and oscillation of the deflector paddle, into and out of the liquid jet forming spray IM, occurred with a mean frequency of 4.89 Hz. Spray IM was disrupted by the deflector paddle for only 13% of the resulting 0.2045 s period; hence the relatively small influence that characteristics of the disrupted jet had on time-averaged data for this spray (see Figure 9). The butterfly sprinkler deflector rotated with an average frequency of 43.56 Hz, producing an outward-moving spiral of droplets with a streamwise spacing of

approximately 255 mm. Smaller droplets in spray B typically travelled more slowly than larger droplets in the spiral, forming a relatively uniform and slow (< 6 m s^{-1}) flow throughout the spray (see Figure 16).

5 Conclusion

The six water sprays that have been experimentally characterised in the present work exhibited a relatively wide variety of spray patterns, droplet sizes and velocities; droplet Sauter mean diameters and characteristic speeds were in the range 240–1,731 μm and 9.1–18.5 m s^{-1}, respectively. Such large differences in spray characteristics could influence the performance of wildfire sprinkler systems significantly. However, previously published investigations have not compared the effectiveness of different sprinklers in these systems. The distributions of water mass flux, droplet diameter and droplet speed reported for each spray in the present work appear to be the first detailed descriptions of these wildfire sprinkler sprays that have been published. Such detailed information will enable the design of sprinkler systems to meet specific performance requirements, and is suitable for the specification of boundary conditions in simulations of wildfire sprinkler systems in future investigations.

The single-camera, high-speed videography technique adopted in the present study proved to be a relatively simple and inexpensive means to obtain individual droplet size and velocity measurements. Droplet equivalent spherical diameters could be measured with a mean absolute error less than 2.9% and 1.3% at the two working distances that were tested, and the focal criterion based on image point-spread function half-width was able to define a distinct measurement volume that was not affected by droplet size. A new method was developed to separate overlapping droplet images by analysing spatial changes in intensity gradient along the combined droplet image boundary. This approach was significantly more effective than existing techniques when applied to the non-spherical droplets that were common in this study.

A detailed account of methods used for videography, image analysis, droplet tracking, and statistical correction for sampling biases have been provided here, to serve as an example of how accurate and detailed spray measurements can be obtained using a single high-speed camera.

Acknowledgements

The authors would like to thank Dr David Hastie and A/Prof Adam Trevitt from the University of Wollongong for their generosity in providing experimental equipment for this study. This research has been conducted with the support of an Australian Government Research Training Program Scholarship to the first author.

References

Bautista-Capetillo, C., Robles, O., Salinas, H. and Playán, E., A Particle Tracking Velocimetry Technique for Drop Characterization in Agricultural Sprinklers, *Irrig. Sci.*, vol. **32**, no. 6, pp. 437–447, 2014. DOI: 10.1007/s00271-014-0440-6

Bautista-Capetillo, C.F., Salvador, R., Burguete, J., Montero, J., Tarjuelo, J.M., Zapata, N., González, J. and Playán, E., Comparing Methodologies for the Characterization of Water Drops Emitted by an Irrigation Sprinkler, *Trans. ASABE*, vol. **52**, no. 5, pp. 1493–1504, 2009.

Blaisot, J.B., Drop Size and Drop Size Distribution Measurements by Image Analysis, *Int. Conf. Liq. At. Spray Syst. ICLASS*, Heidelberg, Germany, 2012.

Blaisot, J.B. and Yon, J., Droplet Size and Morphology Characterization for Dense Sprays by Image Processing: Application to the Diesel Spray, *Exp. Fluids*, vol. **39**, no. 6, pp. 977–994, 2005. DOI: 10.1007/s00348-005-0026-4

Bowman, D.M.J.S., Williamson, G.J., Abatzoglou, J.T., Kolden, C.A., Cochrane, M.A. and Smith, A.M.S., Human Exposure and Sensitivity to Globally Extreme Wildfire Events, *Nat. Ecol. Evol.*, vol. **1**, p. 58, 2017. DOI: 10.1038/s41559-016-0058

Castanet, G., Dunand, P., Caballina, O. and Lemoine, F., High-Speed Shadow Imagery to Characterize the Size and Velocity of the Secondary Droplets Produced by Drop Impacts onto a Heated Surface, *Exp. Fluids*, vol. **54**, no. 3, pp. 1–17, 2013. DOI: 10.1007/s00348-013-1489-3

CFS, CFS Fact Sheet - Sprinkler Systems, South Australian Country Fire Service, 2011.

Dalziel, S.B., Decay of Rotating Turbulence: Some Particle Tracking Experiments, *Appl. Sci. Res.*, vol. **49**, no. 3, pp. 217–244, 1992.

Dalziel, S.B., Digiflow User Guide, DL Research Partners, 2006.

Dorr, G.J., Hewitt, A.J., Adkins, S.W., Hanan, J., Zhang, H. and Noller, B., A Comparison of Initial Spray Characteristics Produced by Agricultural Nozzles, *Crop Prot.*, vol. **53**, pp. 109–117, 2013.

Everest, D. and Atreya, A., Simultaneous Measurements of Drop Size and Velocity in Large-Scale Sprinkler Flows Using Laser-Induced Fluorescence and Mie Scattering, *J. flow Vis. image Process.*, vol. **10**, no. 3–4, pp. 163–181, 2003. DOI: 10.1615/JFlowVisImageProc.v10.i34.10

Fdida, N. and Blaisot, J.B., Drop Size Distribution Measured by Imaging: Determination of the Measurement Volume by the Calibration of the Point Spread Function, *Meas. Sci. Technol.*, vol. **21**, no. 2, p. 15, 2010.

FEMA, Home Builder's Guide to Construction in Wildfire Zones, Federal Emergency Management Agency, Washington, USA, 2008.

FPAA, External Water Spray Systems to Aid Building Protection from Wildfire, Fire Protection Association Australia, 2000.

GTVFD, Sprinkler Protection Systems - Guidelines for Gunflint Trail Fire District, Gunflint Trail Fire Department, 2007.

Guler, H., Zhu, H., Ozkan, H.E., Derksen, R.C., Yu, Y. and Krause, C.R., Spray Characteristics and Drift Reduction Potential with Air Induction and Conventional Flat-Fan Nozzles, *Trans. ASABE*, vol. **50**, no. 3, pp. 745–754, 2007.

Guler, H., Zhu, H., Ozkan, H.E. and Ling, P., Characterization of Hydraulic Nozzles for Droplet Size and Spray Coverage, *At. Sprays*, vol. **22**, no. 8, pp. 627–645, 2012. DOI: 10.1615/AtomizSpr.2012006181

Herráez, J. and Belda, R., Refractive Indices, Densities and Excess Molar Volumes of Monoalcohols + Water, *J. Solution Chem.*, vol. **35**, no. 9, pp. 1315–1328, 2006. DOI: 10.1007/s10953-006-9059-4

ISO, ISO 6182-9:2005 Fire Protection - Automatic Sprinkler System, International Organization for Standardization, Geneva, Switzerland, 2005.

Johnson, J.F., Downing, T. and Nelson, K.C., External Sprinkler Systems and Defensible Space: Lessons Learned from the Ham Lake Fire and the Gunflint Trail, University of Minnesota, College of Food, Agricultural and Natural Resource Sciences, 2008.

Krawchuk, M.A., Moritz, M.A., Parisien, M.A., Van Dorn, J. and Hayhoe, K., Global Pyrogeography: The Current and Future Distribution of Wildfire, *PLoS One*, vol. **4**, no. 4, 2009.

Lee, S.Y. and Kim, Y.D., Sizing of Spray Particles Using Image Processing Technique, *KSME Int. J.*, vol. **18**, no. 6, pp. 879–894, 2004.

Lucas, C., Hennessy, K., Mills, G. and Bathols, J., Bushfire Weather in Southeast Australia: Recent Trends and Projected Climate Change Impacts, Bushfire CRC, Bureau of Meteorology Research Centre, 2007.

Malot, H. and Blaisot, J.-B., Droplet Size Distribution and Sphericity Measurements of Low-

Density Sprays Through Image Analysis, *Part. Part. Syst. Charact.*, vol. **17**, no. 4, pp. 146–158, 2000.

Mitchell, J.W., Wind-Enabled Ember Dousing, *Fire Saf. J.*, vol. **41**, no. 6, pp. 444–458, 2006.

Moritz, M.A., Batllori, E., Bradstock, R.A., Gill, A.M., Handmer, J., Hessburg, P.F., Leonard, J., McCaffrey, S., Odion, D.C. and Schoennagel, T., Learning to Coexist with Wildfire, *Nature*, vol. **515**, no. 7525, pp. 58–66, 2014.

Mugele, R.A. and Evans, H.D., Droplet Size Distribution in Sprays, *Ind. Eng. Chem.*, vol. **43**, no. 6, pp. 1317–1324, 1951.

Myers, T.M. and Marshall, A.W., A Description of the Initial Fire Sprinkler Spray, *Fire Saf. J.*, vol. **84**, pp. 1–7, 2016. DOI: 10.1016/J.FIRESAF.2016.05.004

NFPA, 750: Standard on Water Mist Fire Protection Systems, National Fire Protection Association, Quincy, MA, USA, 2010.

Nuyttens, D., Baetens, K., De Schampheleire, M. and Sonck, B., Effect of Nozzle Type, Size and Pressure on Spray Droplet Characteristics, *Biosyst. Eng.*, vol. **97**, no. 3, pp. 333–345, 2007. DOI: http://dx.doi.org/10.1016/j.biosystemseng.2007.03.001

Potter, M. and Leonard, J., Spray System Design for Ember Attack - Research Findings and Discussion Paper, CSIRO - Sustainable Ecosystems, Bushfire CRC, 2010.

Ren, N., Baum, H.R. and Marshall, A.W., A Comprehensive Methodology for Characterizing Sprinkler Sprays, *Proc. Combust. Inst.*, vol. **33**, no. 2, pp. 2547–2554, 2011. DOI: http://dx.doi.org/10.1016/j.proci.2010.06.107

Salvador, R., Bautista-Capetillo, C., Burguete, J., Zapata, N., Serreta, A. and Playán, E., A Photographic Method for Drop Characterization in Agricultural Sprinklers, *Irrig. Sci.*, vol. **27**, no. 4, pp. 307–317, 2009. DOI: 10.1007/s00271-009-0147-2

Santangelo, P.E., Characterization of High-Pressure Water-Mist Sprays: Experimental Analysis of Droplet Size and Dispersion, *Exp. Therm. Fluid Sci.*, vol. **34**, no. 8, pp. 1353–1366, 2010. DOI: http://dx.doi.org/10.1016/j.expthermflusci.2010.06.008

Sheppard, D.T. and Lueptow, R.M., Characterization of Fire Sprinkler Sprays Using Particle Image Velocimetry, vol. **15**, no. 3, pp. 341–362, 2005. DOI: 10.1615/AtomizSpr.v15.i3.50

Sidahmed, M.M., Taher, M.D. and Brown, R.B., A Virtual Nozzle for Simulation of Spray Generation and Droplet Transport, *Biosyst. Eng.*, vol. **92**, no. 3, pp. 295–307, 2005. DOI: http://dx.doi.org/10.1016/j.biosystemseng.2005.07.012

Standards Australia, AS 4587-1999: Water Mist Fire Protection Systems, 1999.

Standards Australia, AS 5414-2012: Bushfire Water Spray Systems, 2012.

Syphard, A.D., Massada, A.B., Butsic, V. and Keeley, J.E., Land Use Planning and Wildfire: Development Policies Influence Future Probability of Housing Loss, *PLoS One*, vol. **8**, no. 8, 2013.

Vazquez, G., Alvarez, E. and Navaza, J.M., Surface Tension of Alcohol Water + Water from 20 to 50 .Degree.C, *J. Chem. Eng. Data*, vol. **40**, no. 3, pp. 611–614, 1995. DOI:

10.1021/je00019a016

Vulgarakis Minov, S., Cointault, F., Vangeyte, J., Pieters, J. and Nuyttens, D., Spray Droplet Characterization from a Single Nozzle by High Speed Image Analysis Using an In-Focus Droplet Criterion, *Sensors*, vol. **16**, no. 2, p. 218, 2016.

Widmann, J., Sheppard, D. and Lueptow, R., Non-Intrusive Measurements in Fire Sprinkler Sprays, *Fire Technol.*, vol. **37**, no. 4, pp. 297–315, 2001. DOI: 10.1023/A:1012727614590

Yoon, S.H., Kim, D.Y., Kim, D.K. and Kim, B.H., Effect of Nozzle Geometry for Swirl Type Twin-Fluid Water Mist Nozzle on the Spray Characteristic, *J. Mech. Sci. Technol.*, vol. **25**, no. 7, pp. 1761–1766, 2011. DOI: http://dx.doi.org/10.1007/s12206-011-0506-9

Yoon, S.S., Kim, H.Y. and Hewson, J.C., Effect of Initial Conditions of Modeled PDFs on Droplet Characteristics for Coalescing and Evaporating Turbulent Water Spray Used in Fire Suppression Applications, *Fire Saf. J.*, vol. **42**, no. 5, pp. 393–406, 2007. DOI: http://dx.doi.org/10.1016/j.firesaf.2007.01.001

You, H.Z., Investigation of Spray Patterns of Selected Sprinklers with the FMRC Drop Size Measuring System, *Fire Saf. Sci.*, vol. **1**, pp. 1165–1176, 1986.

Zhou, X., D'Aniello, S. and Yu, H.-Z., Spray Measurements of an Upright Fire Sprinkler, *Fire Technol.*, vol. **50**, no. 3, pp. 457–482, 2014. DOI: 10.1007/s10694-012-0314-5

Zhou, X., D'Aniello, S.P. and Yu, H.-Z., Spray Characterization Measurements of a Pendent Fire Sprinkler, *Fire Saf. J.*, vol. **54**, no. 0, pp. 36–48, 2012. DOI: http://dx.doi.org/10.1016/j.firesaf.2012.07.007

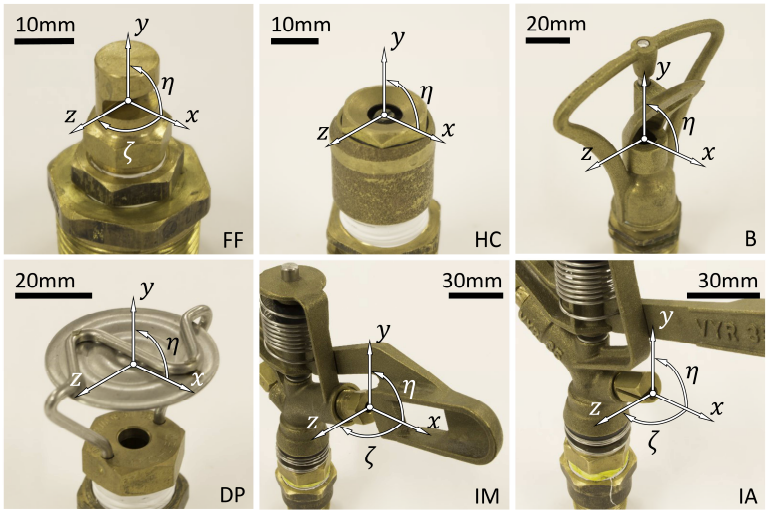

Figure 1: Images of the flat-fan spray nozzle (FF); hollow-cone nozzle (HC); butterfly sprinkler (B); deflector-plate sprinkler (DP); impact sprinkler main nozzle (IM); and impact sprinkler auxiliary nozzle (IA). Cartesian coordinates (x, y and z) and spherical coordinates (elevation angle, η, and azimuthal angle, ζ) have been shown, where applicable.

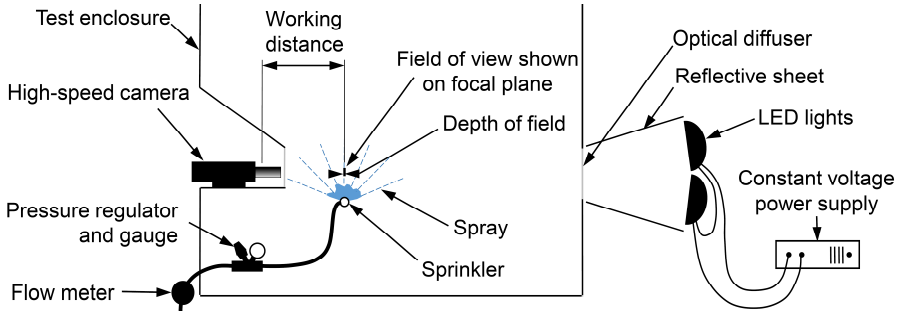

Figure 2: Cross-section of the experimental setup used for spray videography.

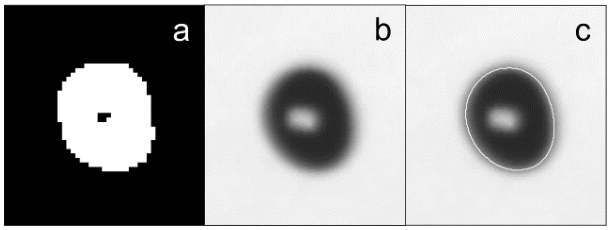

Figure 3: Preliminary treatment of a 'blob', corresponding to a droplet image. Steps included: a) segregation of a region surrounding the blob; b) sub-pixel interpolation of the corresponding droplet image; and c) definition of the droplet image boundary.

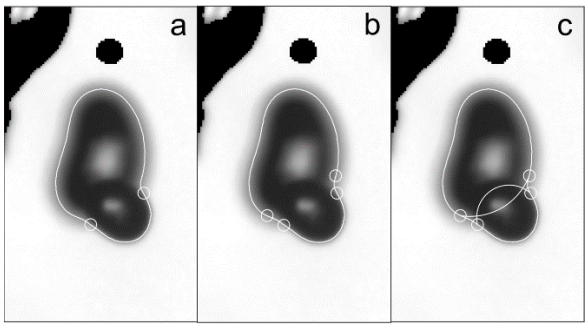

Figure 4: Detection and separation of overlapping droplet images, based on the intensity gradient at the image boundary. Steps in the process included: a) identification of potential 'break points' on the image boundary; b) definition of secondary break points, translated towards the image that was in poorer focus; and c) completion of each droplet boundary with arcs.

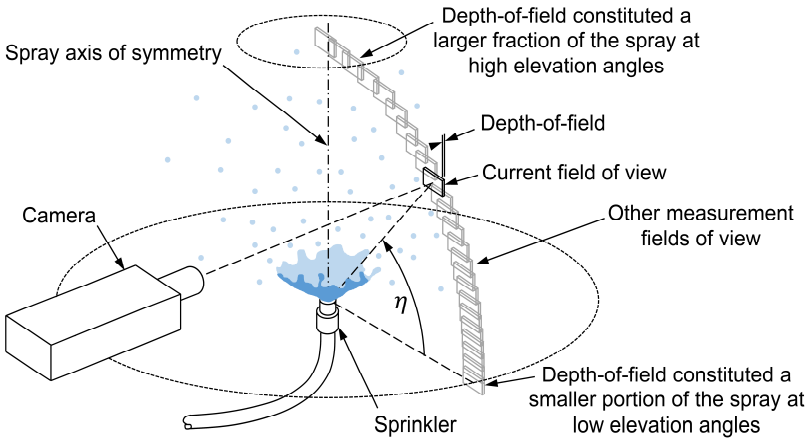

Figure 5: Geometry of measurements of axisymmetric sprays, which introduced an inherent bias towards droplets close to the axis of symmetry.

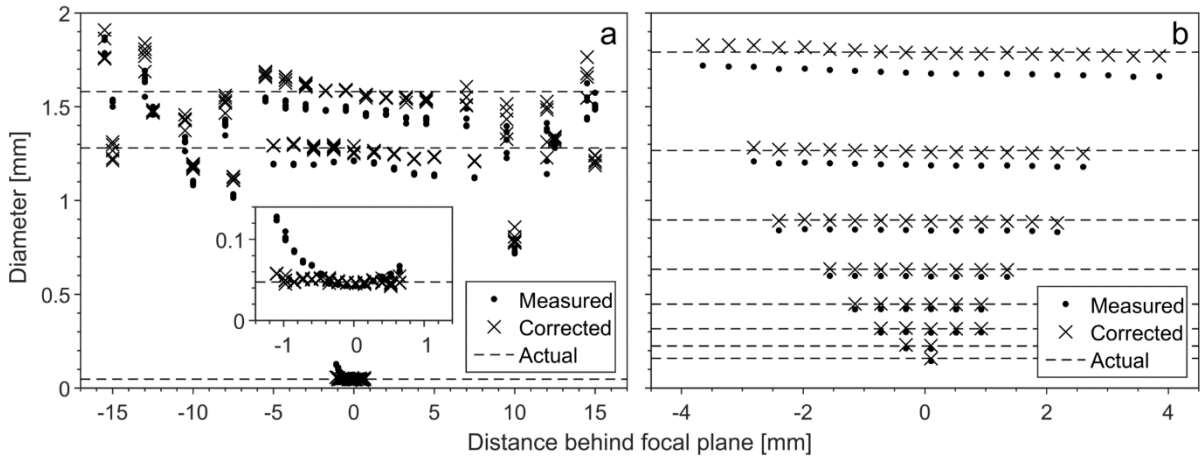

Figure 6: Calibration results showing the measured, corrected and actual diameters of a) droplets and b) opaque discs, at various distances from the focal plane. Data presented here is for a working distance of 122 mm. The inset in 'a' shows a magnified view of data in the lower part of the figure.

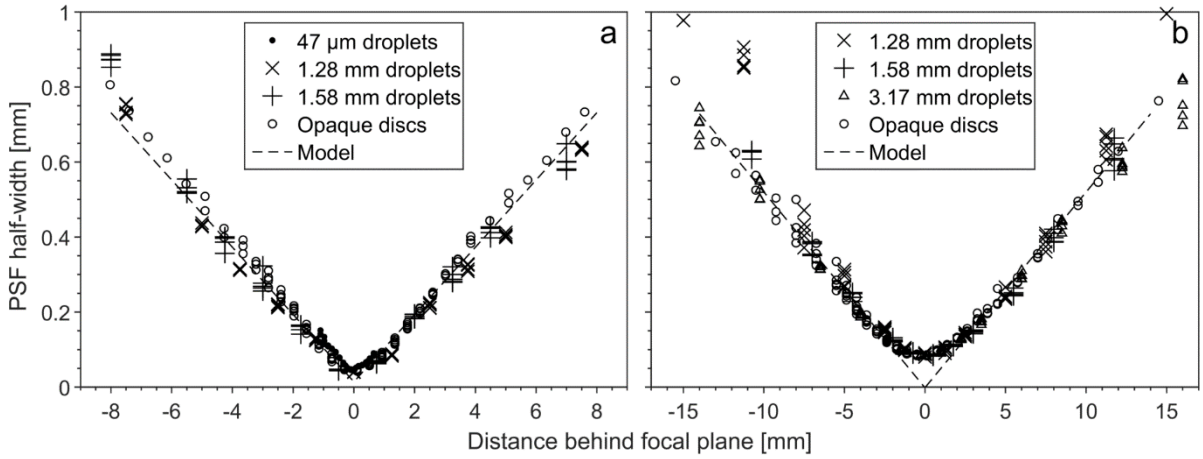

Figure 7: Relationship between the point-spread function (PSF) half-width of images and the distance of the imaged object from the focal plane, at working distances of a) 122 mm, and b) 247 mm.

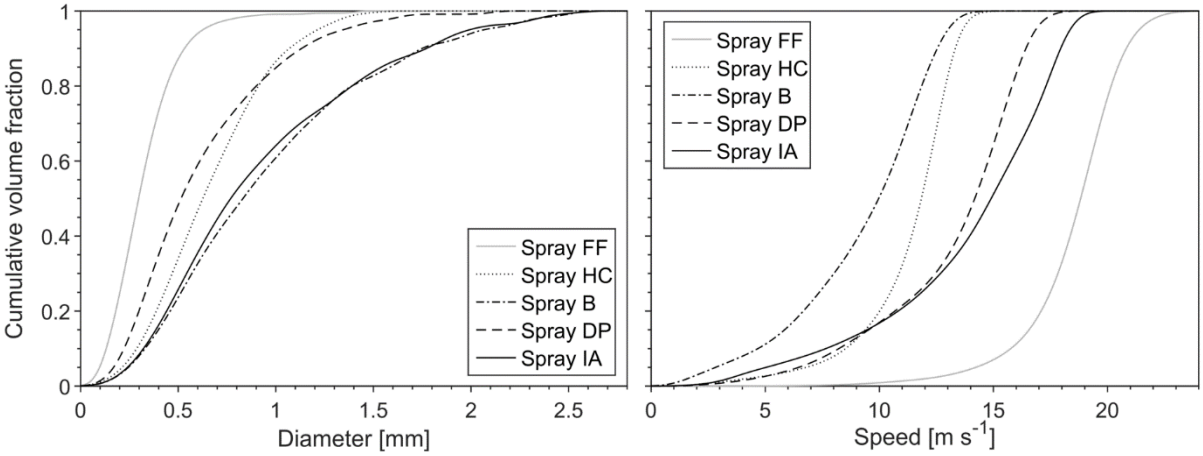

Figure 8: Comparison of droplet diameter and speed marginal distributions in 5 of the 6 sprays.

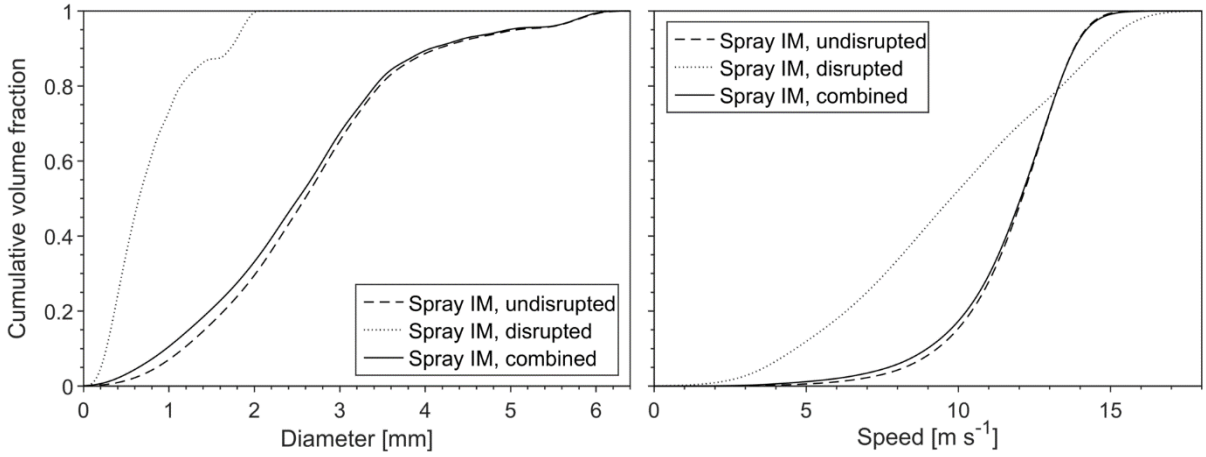

Figure 9: Comparison of droplet diameter and speed distributions in spray IM. Separate distributions have been plotted representing the spray formed from the liquid jet when disrupted or not disrupted by the rotating deflector paddle, as well as the combined (i.e. time-averaged) distributions.

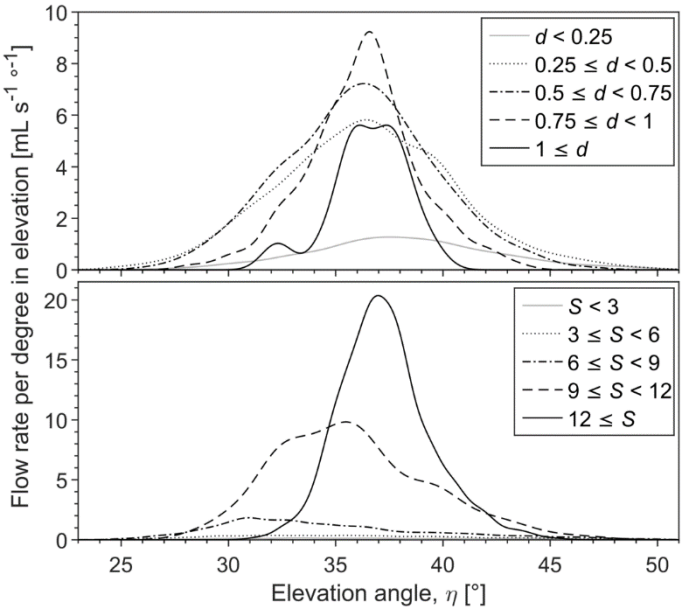

Figure 10: Spatial distributions of the liquid volume flux, 326 mm from the hollow-cone nozzle, for a number of discrete diameter (d mm) and speed (S m s^{-1}) classes.

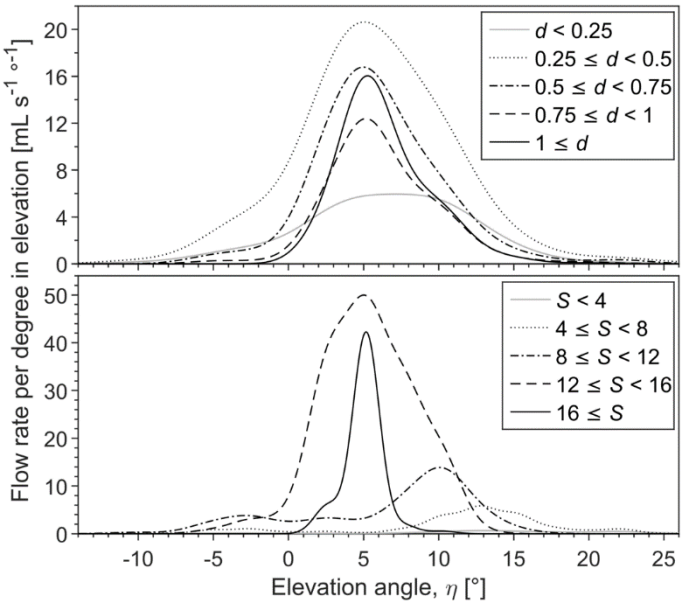

Figure 11: Spatial distributions of the liquid volume flux, 221 mm from the deflector-plate sprinkler, for a number of discrete diameter (d mm) and speed (S m s^{-1}) classes.

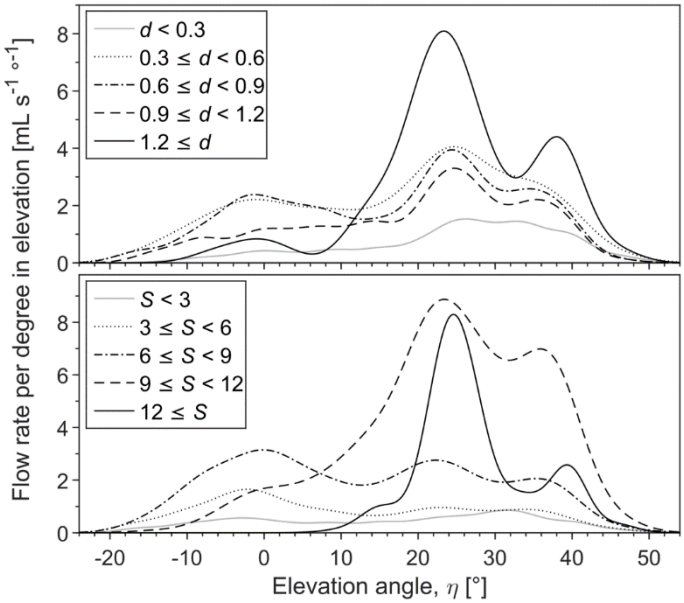

Figure 12: Spatial distributions of the liquid volume flux, 533 mm from the butterfly sprinkler, for a number of discrete diameter (d mm) and speed (S m s^{-1}) classes.

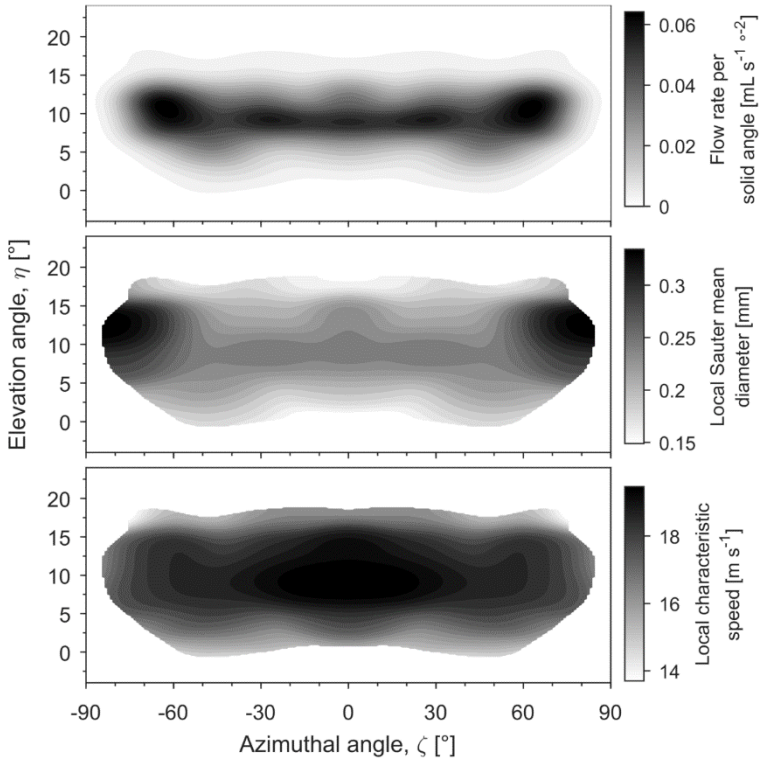

Figure 13: Spatial distributions of liquid volume flux, local Sauter mean diameter and local characteristic speed, 100 mm from the flat-fan nozzle (in spray FF).

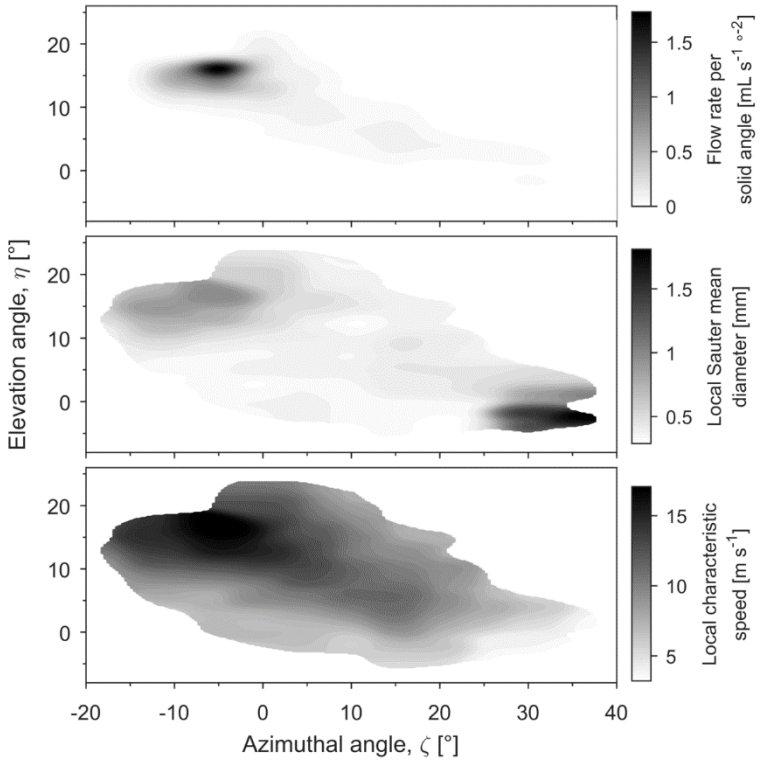

Figure 14: Spatial distributions of liquid volume flux, local Sauter mean diameter and local characteristic speed in spray IA, 536 mm from the impact sprinkler auxiliary nozzle. The sprinkler was restrained during measurement, to prevent rotation about the y-axis.

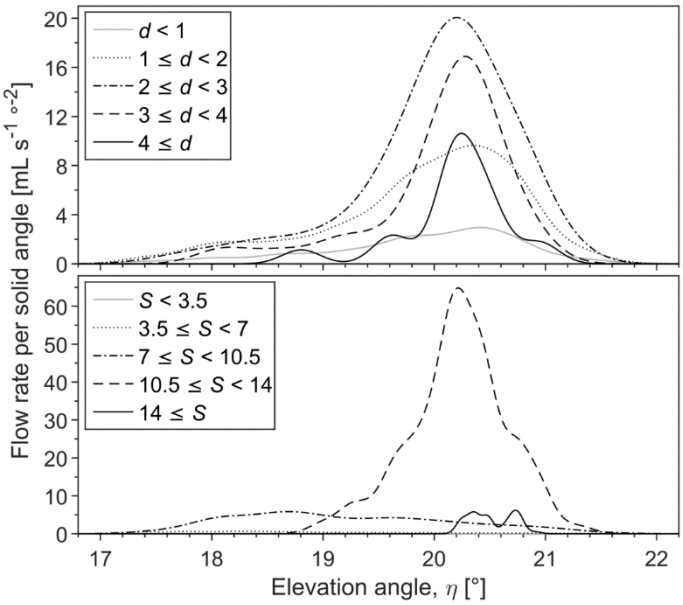

Figure 15: Spatial distributions of liquid volume flux through the vertical centre plane of spray IM when undisrupted by the deflector paddle, measured 6 m from the sprinkler. The sprinkler was inclined forward by 15° and prevented from rotating about the y-axis during measurement.

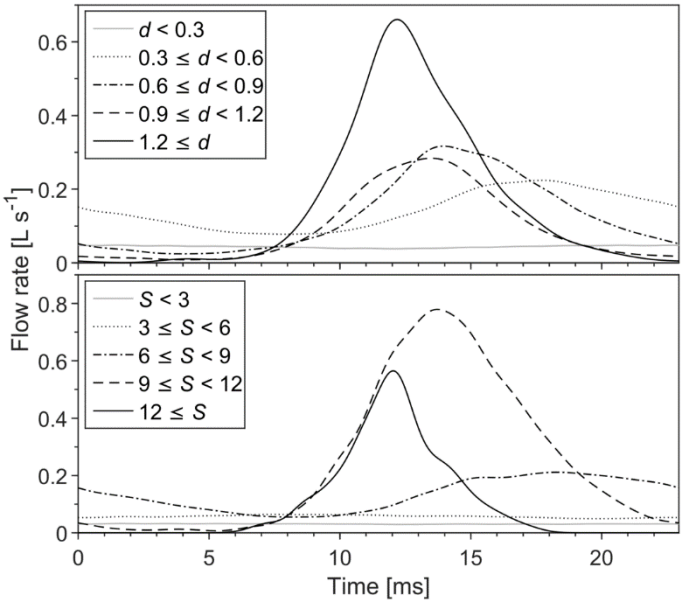

Figure 16: Temporal variations in spray B, measured at a fixed azimuthal angle ($\zeta = 0$), 533 mm from the sprinkler, and plotted for time period corresponding to one rotation of the sprinkler deflector. Results are expressed in terms of the volume flow rate of droplets within discrete diameter (d mm) and speed (S m s^{-1}) classes.

Table 1: Details of the sprays that were characterised.

Spray	Sprinkler model	Pressure [kPa]	Flow rate [L min^{-1}]
FF	Tecpro KHW-1390 180° deflector flat-fan nozzle	400	4.1
HC	½-inch Champion S9F hollow-cone nozzle	345	12.5
B	Holman ½-inch brass butterfly sprinkler	200	34
DP	Lechler 525.049 deflector-plate sprinkler	245	41.8
IM	Vyrsa VYR 35 ¾-inch 360° impact sprinkler main nozzle	250	17.4
IA	Vyrsa VYR 35 ¾-inch 360° impact sprinkler auxiliary nozzle	250	5.4

Table 2: Test conditions set for each spray. Sprays were produced using the flat-fan nozzle (FF), hollow-cone nozzle (HC), deflector-plate sprinkler (DP), butterfly sprinkler (B), impact sprinkler auxiliary nozzle (IA) and impact sprinkler main nozzle (IM).

	FF	HC	B	DP	IA	IM	
						Disrupted	Undisrupted
Working distance [mm]	122	122	247	247	247	247	247
Resolution [pixels mm-1]	50.53	50.53	22.42	22.42	22.42	22.42	22.42
Field of view (width; height) [mm]	13.9; 13.9	25.3; 15.8	57.1; 35.7	57.1; 35.7	57.1; 35.7	57.1; 35.7	57.1; 35.7
Frame rate [frames s-1]	11,104	6,273	6,273	6,273	6,273	6,273	6,273
Exposure period [μs]	4	7	7	5	4	5	6
Measurement distance from nozzle [mm]	100	326	533	221	536	300	6,000
Assumed axis of symmetry	xy-plane	y-axis	y-axis	y-axis	-	-	-
Number of regions videoed	160	23	24	22	74	12	20

Table 3: Characteristics of the sprays investigated. Four common functional forms were trialled on the spray data, including the Rosin-Rammler distribution, log-normal distribution, upper-limit log-normal distribution (ULLN) and a hybrdid log-normal/Rosin-Rammler distribution (LN/RR); the functions that best fit each dataset are presented here, with the relevant parameters.

	FF	**HC**	**B**	**DP**	**IA**	**IM**		
						Disrupted	**Undisrupted**	**Combined**
Measurement distance from nozzle [mm]	100	326	533	221	536	300	6,000	-
Number of droplets measured ($\times 10^3$)	155	91	343	120	160	18	29	47
Arithmetic mean diameter, d_{10} [µm]	102	122	183	176	196	219	336	273
Volume mean diameter, d_{30} [µm]	159	263	341	273	354	336	912	720
Volume-length mean diameter, d_{31} [µm]	199	387	465	340	475	416	1,504	1,168
Sauter mean diameter, d_{32} [µm]	240	496	615	419	610	517	2,002	1,731
Best functional fit to diameter distribution	LN/RR	ULLN	ULLN	ULLN	LN/RR	-	-	-
Size parameter for LN/RR or ULLN function	0.2899	0.9039	0.9917	0.5133	0.7496	-	-	-
Distribution parameter for LN/RR or ULLN function	2.0163	2.1388	2.3027	1.9147	1.4825	-	-	-
Maximum size parameter for ULLN function	-	1.9114	4.3431	21.5965	-	-	-	-
Mean characteristic speed [m s^{-1}]	18.5	11.3	9.1	13.2	13.9	9.7	11.8	11.7